Optical Engineering

OpticalEngineering.SPIEDigitalLibrary.org

Infrared computer-generated holograms: design and application for the WFIRST grism using wavelength-tuning interferometry

Margaret Z. Dominguez
Catherine T. Marx
Qian Gong
John G. Hagopian
Ulf Griesmann
James H. Burge
Dae Wook Kim

SPIE.

Margaret Z. Dominguez, Catherine T. Marx, Qian Gong, John G. Hagopian, Ulf Griesmann, James H. Burge, Dae Wook Kim, "Infrared computer-generated holograms: design and application for the WFIRST grism using wavelength-tuning interferometry," *Opt. Eng.* **57**(7), 074105 (2018), doi: 10.1117/1.OE.57.7.074105.

Infrared computer-generated holograms: design and application for the WFIRST grism using wavelength-tuning interferometry

Margaret Z. Dominguez,[a,b,*] Catherine T. Marx,[a] Qian Gong,[a] John G. Hagopian,[c] Ulf Griesmann,[d] James H. Burge,[b] and Dae Wook Kim[b,e,*]
[a]NASA Goddard Space Flight Center, Greenbelt, Maryland, United States
[b]University of Arizona, College of Optical Sciences, Tucson, Arizona, United States
[c]ATA Aerospace, Albuquerque, New Mexico
[d]National Institute of Standards and Technology, Physical Measurement Laboratory, Gaithersburg, Maryland, United States
[e]University of Arizona, Department of Astronomy and Steward Observatory, Tucson, Arizona, United States

Abstract. Interferometers using computer-generated holograms (CGHs) have become the industry standard to accurately measure aspheric optics. The CGH is a diffractive optical element that can create a phase or amplitude distribution and can be manufactured with low uncertainty using modern lithographic techniques. However, these CGHs have conventionally been used with visible light and piezo-shifting interferometers. Testing the performance of transmissive optics in the infrared requires infrared CGHs and an infrared interferometer. Such an instrument is used in this investigation, which introduces its phase shift via wavelength-tuning. A procedure on how to design and manufacture infrared CGHs and how these were successfully used to model and measure the Wide-Field Infrared Survey Telescope grism elements is provided. Additionally, the paper provides a parametric model, simulation results, and calculations of the errors and measurements that come about when interferometers introduce a phase variation via wavelength-tuning interferometry to measure precision aspheres. [DOI: 10.1117/1.OE.57.7.074105]

Keywords: optical testing; computer-generated hologram; infrared; wavelength-tuning; interferometry; grism; diffractive optical elements.

Paper 180618 received Apr. 29, 2018; accepted for publication Jun. 26, 2018; published online Jul. 14, 2018.

1 Introduction

Wide-Field Infrared Survey Telescope (WFIRST) is a NASA observatory that will study dark energy, exoplanets, and infrared astrophysics. WFIRST has a primary mirror that is 2.4 m (7.9 feet) in diameter, the same size as the Hubble Space Telescope's (HST) primary mirror. WFIRST will have two instruments: the wide-field instrument[1] and the coronagraph instrument.[2] The telescope will have a field-of-view (FoV) about 90 times bigger than the HST and ∼200 times larger than the HST IR channel of wide-field camera 3. This capability will enable the telescope to capture more of the sky with less observing time, allowing WFIRST to measure light from a billion galaxies over the course of its 6 year lifetime. While Hubble has found only a few galaxies within 500 million years of the Big Bang, WFIRST is expected to find hundreds.[3]

The scientific objectives of the wide-field instrument are to answer two fundamental questions: (1) is cosmic acceleration caused by an energy component or by a breakdown of general relativity? and (2) if the cause is an energy component, is its energy density constant in space and time or has it evolved over the history of the universe? To answer these questions, WFIRST will conduct three different types of surveys, which are: type la supernovae survey, high-latitude spectroscopy survey, and high-latitude imaging survey. This last survey will measure accurate distances and positions of numerous galaxies, allowing us to measure the growth of the universe. It will also measure the redshifts of tens of millions of galaxies via slitless spectroscopy, utilizing a grism (combination of a grating and a prism) to survey the distribution of emission line galaxies. The predicted number of emitting galaxies in 2014 was estimated to be 20 million, meaning that the grism survey is expected to discover thousands of luminous quasars, whose existence tracks the assembly of billion solar mass black holes a few hundred million years after the Big Bang. The grism, by slitless spectroscopy, will allow the surveying of a large section of the sky (about thousands of square degrees, where the whole sky is ∼27,000 square degrees) to find bright galaxies.[4]

1.1 *WFIRST Grism Prototype Design*

The first design version of the grism was a three-element system, as shown in Fig. 1. It consists of three lens elements with diffractive surfaces on two of the elements, element 1 (on surface 2) and element 3 (on surface 2). It has a spectral range of 1.35 to 1.95 μm. The designed grism wavefront error (WFE) satisfies its diffraction-limited performance across the wavelength band. Even though each individual element is highly aberrated, they become diffraction-limited due to the compensations among them when assembled. The main challenges with the grism are the optical design due to

*Address all correspondence to: Margaret Z. Dominguez, E-mail: margaret.z.dominguez@nasa.gov; Dae Wook Kim, E-mail: letter2dwk@hotmail.com

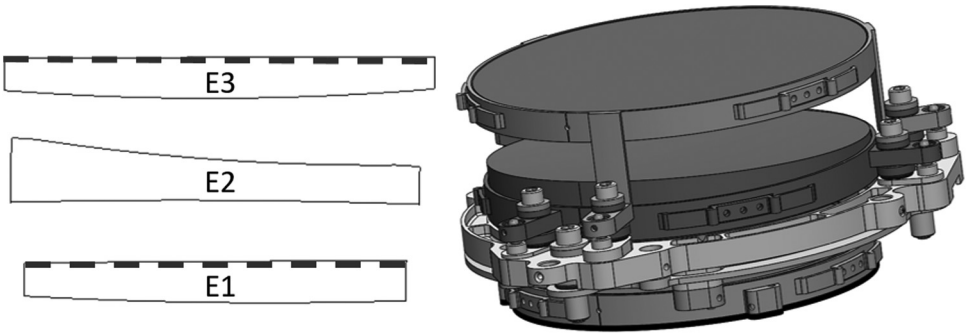

Fig. 1 (a) Optical layout of the grism prototype, indicating the diffractive pattern (dashed line) on the flat surfaces of E1 and E3. (b) Three-dimensional solid CAD model of the grism with optomechanical structure.

its wide FoV, large dispersion, and relatively small f-number, and fabrication of high-efficiency diffractive surfaces.[5–7]

Each of the elements was made of fused silica (Corning 7980$^+$. Element 1 (E1) is wedged with a spherical front surface and a flat back surface that has a diffractive pattern on it. The function of E1 is to correct the wavelength scaled aberration from the gratings being used in noncollimated space. Element 2 (E2) is also wedged and biconcave. The function of E2 is to deviate the beam to make the assembly zero deviation. Element 3 (E3), similar to E1, has a spherical front surface and flat back surface with a diffractive pattern on it but does not have a wedge. The function of E3 is to provide the required spectral dispersion for the instrument. To measure each element in transmission, a separate computer-generated hologram (CGH) was designed and manufactured. The detailed design strategy and procedure are presented in Sec. 2. Table 1 shows the grism prototype specifications.

1.2 *Wavelength-Tuning Infrared Interferometry*

Binary CGHs are widely used for testing advanced optics like aspheres, freeforms, or those with grating patterns on them. However, working with them comes with a few disadvantages, such as unwanted diffraction orders. These unwanted orders form ghost fringes, which reduce measurement uncertainty if not fully blocked. They also reduce fringe contrast. These disadvantages can mostly be overcome by separating the diffraction orders by adding carriers, either a tilt carrier for lateral separation or a power carrier for longitudinal separation. In the CGH design process, where the wanted order is often the first order, efforts were made to eliminate the ghost fringes from the unwanted orders as best as possible.[8]

Table 1 WFIRST grism prototype specifications.

Wavelength range (μm)	1.35 to 1.95
FoV (deg)	0.788×0.516
Beam diameter at grism (mm)	120
Beam $f/\#$ at grism	$\sim f/8$
WFE	Diffraction limited at 1.65 μm
Minimum dispersion length (mm)	>4.91
Size	70-mm total thickness

For decades, binary CGHs and interferometers have successfully been used to measure aspheres. However, conventional phase-shifting infrared interferometers can have limitations because they require moving a reference surface. An alternative to this conventional method is phase-shifting via wavelength-tuning, which provides a smooth and repeatable optical phase variation without the need to physically move any components within the optical cavity. It allows a simpler test setup and reduces susceptibility to external vibrations on phase measurements. Also, using a wavelength-tuning interferometer can remove the need of having the interferometer on a floating table, allowing measurements in not necessarily stable environments.[9]

A basic layout of an interferometer configured to test a flat using wavelength-tuning for phase shifting is shown in Fig. 2. The interferometer cavity is defined by the reference flat together with the test optic. For a cavity of length L with a refractive index n and a specific wavelength λ, the difference in phase between the test and reference beams is as follows:[9]

$$\varphi = \phi_T - \phi_R = 2\frac{2\pi}{\lambda}Ln = \frac{4\pi Ln}{c}\nu, \tag{1}$$

where ν is the optical frequency and c is the speed of light. If the cavity length and index are fixed, the variation in optical path (phase) as a function of optical frequency change is as follows:

$$\frac{\partial\varphi}{\partial t} = 2\pi\frac{2Ln}{c}\frac{\partial\nu}{\partial t}. \tag{2}$$

Therefore, the phase variation has a linear dependence with the optical frequency variation and a factor proportional to cavity length. With phase-shifting interferometers, images are collected while the phase is varied at a constant rate with, e.g., a 90-deg phase increment. Depending on the phase extraction algorithm, the number of images collected is typically five or seven.[8] Equation (2) implies that the frequency change necessary to produce the required phase change will

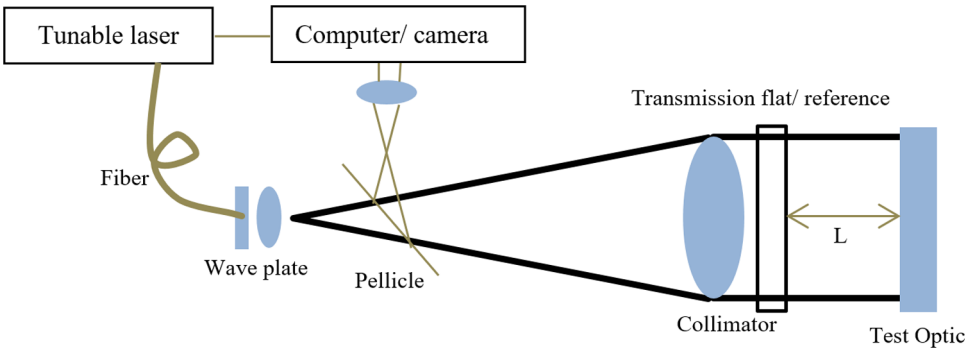

Fig. 2 Schematic wavelength-tuning interferometer layout with a cavity length *L*.

be inversely proportional to the cavity length. The frequency variation is accomplished with a tunable laser source.[10]

Section 2 describes the design and manufacturing process of a phase CGH that is used to test the individual elements of the WFIRST grism prototype. Section 3 presents a parametric model, which will show various wavefront phase sensitivity functions, including the one associated with wavelength. Since our interferometer used a wavelength-tuning technique to introduce the phase shift, the impact of varying the wavelength on a phase type CGH needs to be quantitatively investigated, modeled, and predicted. The same concern extends to the diffractive elements of the grism. This will be done by calculating the sensitivity and error associated with wavelength-tuning for infrared CGHs and comparing that to the simulated results of the CGHs designed and manufactured to measure the WFIRST grism elements E1 and E3. Finally, Sec. 4 presents the experimental results obtained with the independent elements of the WFIRST grism prototype. The measured results will be discussed, including a comparison of measurements done using a conventional piezo-shifting technique and a wavelength-tuning one, both in the infrared. Finally, Sec. 5 summarizes our findings.

2 Infrared CGHS Design Strategy for WFIRST Grism Metrology

The infrared CGHs that used to measure the transmitted WFE of the WFIRST grism elements were designed at Goddard Space Flight Center and manufactured at the NIST Center for Nanoscale Science and Technology. The comprehensive design approach is stated in this section for the retrace-ability of the presented work.

The process started with a Zemax$^+$ (raytracing software) model of each independent grism element in collimated space. The grism has a broad wavelength range (1.35 to 1.95 μm). A wavelength close to the center of the range is a good starting point, 1.55 μm. Since this is the fiber communications C-band wavelength, it is easier to find it on interferometers. The interferometer used had 1.55 μm as its operating wavelength. A CGH substrate was placed at a specific distance in front of each of the individual grism elements in collimated space, as shown in Fig. 3. The advantage of having the CGH in collimated space was the insensitivity to the placement of the CGH relative to the interferometer in translation; tip/tilt still needs to be controlled.

It is important to keep in mind that in order to make a working design, a good quality substrate must be used. Depending on the error requirement, it is important to start with either a high-optical quality substrate or to measure a lesser quality one prior to writing on it, and introduce the measured imperfections into the model or calibrate them out at their zero-order after measuring. For grism prototype testing, in which results are discussed in Sec. 4, we used a lower-quality CGH substrate and proceeded to calibrate its zero-order out.

A flat mirror was added after the grism element, setting its tip/tilt angle to be variable. Immediately after the CGH glass surface, a Zernike fringe phase type surface was added. The Zernike fringe phase surface in Zemax$^+$ can be used to model some holograms and binary optics surfaces. The phase of the surface is given by

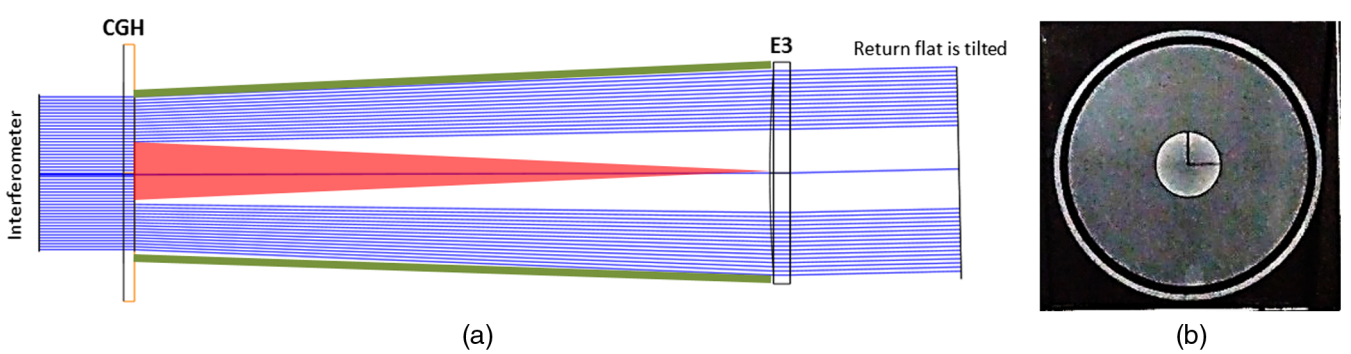

Fig. 3 (a) Zemax$^+$ layout of the CGH and its three different sections used to measure E3. From left to right includes the interferometer with its transmission flat, collimated space, the CGH, diverging space, E3 grism element, collimated space, and return flat. (b) Final phase CGH made for testing the E3 grism element, with three sections: main, retro, and ring fiducial. It includes additional orientation features contained inside the retro section in the center.

$$\Phi = 2\pi M \sum_{i=1}^{N} A_i Z_i(\rho, \varphi), \tag{3}$$

where N is the number of the Zernike coefficients in the series, A_i is the coefficient of the i'th Zernike fringe polynomial, ρ is the normalized radial ray coordinate, φ is the angular ray coordinate, and M is the diffraction order.[11]

The parameters of the Zernike fringe phase type surface of the CGH were specified, including the diffraction order, the number of Zernike terms, and the normalization radius, all of which are indicated in Table 2.

Up to 21 Zernike coefficients[12] were set to be variable and optimized to create the null testing condition. Figure 4 shows the designed phase maps of the CGH main section used for measuring the grism elements E1 and E3. The shape for the phase maps indicates a high amount of power, Z4, which is consistent with the values listed in Table 2, where the power term is the dominant Zernike coefficient value.

Table 2 E1 and E3 main (i.e., testing) CGH section specifications, where the Zernike fringe coefficients (RMS normalization) are in waves at 1550 nm.

	E1	E3
Diffraction order	1	1
Normalization radius (mm)	55	60
Z1 (waves)	0	0
Z2 (waves)	0	0
Z3 (waves)	100.00000	100.00000
Z4 (waves)	153.39081	488.97245
Z5 (waves)	27.84660	−52.76998
Z6 (waves)	−1.67776	3.19355
Z7 (waves)	0.01360	−0.11743
Z8 (waves)	11.08712	−28.28801
Z9 (waves)	0.16952	1.96446
Z10 (waves)	−0.02739	0.14608
Z11 (waves)	0.30601	1.19632

Note: Only the first 11 Zernike coefficients are listed here.

After the main CGH section was designed, alignment aids and fiducial sections were designed and added to the multi-pattern CGH. There were three sections: the main pattern, the retro in the center that used about 5% to 10% of the surface area of the CGH pattern, and a 6-mm-wide ring fiducial surrounding the main section. Both the retro and the ring sections work with the interferometer's visible alignment aid light, so they were designed to work at 632.8 nm. Figure 3(a) shows the Zemax$^+$ layout of the CGH measuring E3 with its three different sections in different colors. The retro section, which focuses at the center first surface of the grism element, is shown in red, and the ring fiducial forming a visible ring around the clear aperture of the element is shown in green. The main section is shown in blue. Additional alignment aids were added to the retro section pattern to define orientation. Figure 3(b) shows the entire CGH pattern with various CGH sections and alignment aids. During the optimization process, care was taken to ensure that there was no overlap of various diffraction orders at the image plane in the main section of the CGH. This was done by adding tilt and/or power carriers to the design. Since the first order was the designed order, the zeroth order and +3 order had to be carefully monitored. If various orders overlapped each other, this could contribute to detrimental ghost fringes.

The optimized Zernike coefficients along with the normalization radius values were converted into a graphic data system (GDS) type format file for processing with a laser writer. The GDS file was written by the laser writer onto a 6 in. × 6 in. quartz photomask with chrome and resist. After chrome etching, an interim amplitude CGH pattern on the substrate was created. However, the grism elements E1 and E3 have diffractive optical elements, making phase type CGHs necessary. Therefore, an etch depth value was calculated, ∼1.7-μm deep. This was achieved using a reactive ion plasma etcher.[13] Afterward, the depth was verified to meet the specification to within 10%. The final product is shown in Fig. 3(b).

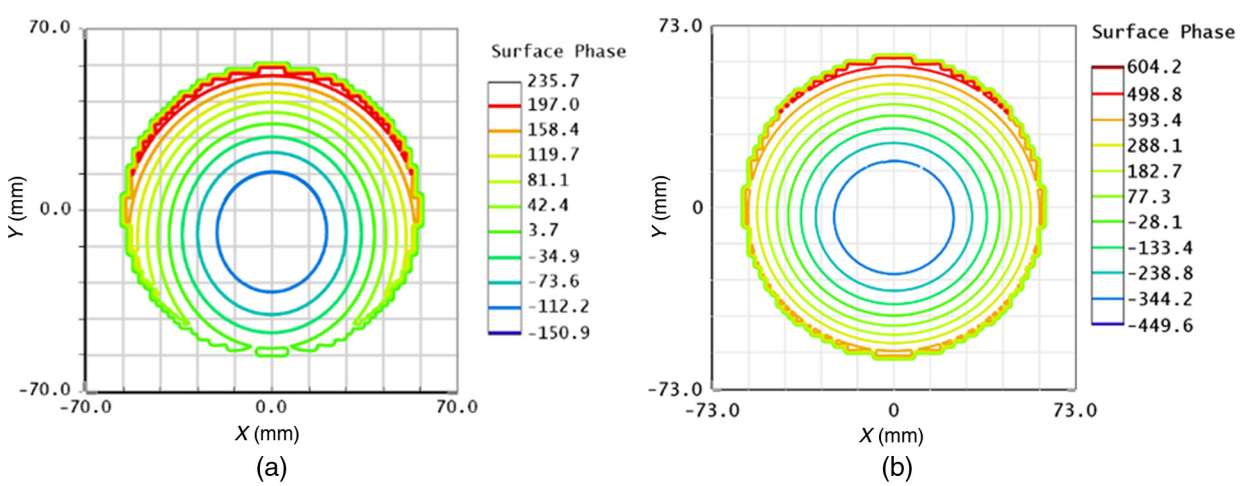

Fig. 4 Surface phase map of main CGH section for (a) E1 and (b) E3. Phase is in units of periods, one period represents a phase change of 2π.

Unlike the visible light CGH design process, the alignment features that would normally be visible are no longer available, making the design and alignment of these CGHs more challenging when using an IR-only interferometer. If a visible and IR interferometer is available, sections like the retro and ring features can be used.

3 Infrared CGH Wavefront Error Analysis

3.1 *Parametric Phase CGH Wavefront Error Sensitivity Model*

There are two types of CGHs used for optical testing: amplitude and phase. The first one often consists of a chromium pattern written on high-quality optical glass, and the latter is such a pattern etched into the glass. Most CGHs are a combination of the two types, however, phase CGHs provide a much higher diffraction efficiency, which may be required for testing bare-glass surfaces in a double pass setup. Binary phase CGHs can have up to 40.5% [13,14] diffraction efficiency at the first orders, much greater than binary amplitude CGHs, making them useful then testing with low-fringe contrast. When considering either CGH types, the substrate on which this CGH is made can have errors. To measure these substrate errors, we start by measuring the zero-diffraction order, and later subtract it from the nonzero order measurement.

Zhou, Zhao, and Burge[15,16] have discussed various manufacturing and test errors associated with the use of a phase CGH, such as the sensitivities associated with duty cycle, etch depth, and amplitude variation. We expand on this work to include the calculation of the sensitivity associated with wavelength variation and the effect it has on the phase of a CGH when measuring an optic using of wavelength-tuning interferometry. Scalar diffraction theory assumes that the wavelength of incident light on a CGH is much smaller than the grating period S, as shown in Fig. 5, while in our case, the period was about 100 μm. When using a wavelength-tuning interferometer, the shift of the wavelength can be assumed to be small, no more than single-digit nanometers, but ultimately depend on the cavity length, as shown in Sec. 4, which continues to be consistent with scalar diffraction theory. During testing, it is assumed that the grating is illuminated with a wavefront at normal incidence. Figure 5 illustrates a surface profile of a binary phase CGH grating, assuming that the light is propagating from the bottom upward. This grating has a period S and an etch depth t. The duty cycle is defined as $D = b/S$, where b is the width of the unetched area. The A_0 and A_1 coefficients represent the amplitudes of the output wavefront from the unetched and etched areas of the grating, respectively. The phase difference between the rays from the peaks and valleys represents the phase function of the grating structure in transmission. For a phase-type CGH used in transmission, A_0 and A_1 are approximately unity.

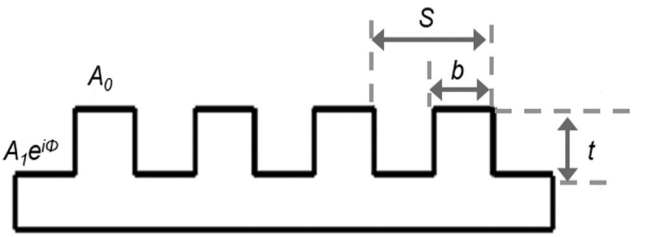

Fig. 5 Schematic binary linear surface profile of a phase CGH.

The wavefront phase sensitivity functions are calculated from the wavefront phase function. It is approximated as $\tan\Psi \approx \Psi$ due to the assumption that Ψ is sufficiently small. The zero and nonzero m'th order wavefront phase functions are as follows:

$$\Psi = \begin{cases} \frac{A_1 D \sin\Phi}{A_0(1-D)+A_1 D\cos\Phi}, & m = 0, \\ \frac{A_1 \sin\Phi \sin c(mD)}{(-A_0+A_1\cos\Phi)\sin c(mD)}, & m \neq 0, \end{cases} \tag{4}$$

and its sensitivity functions can be evaluated directly to be $\frac{\partial\Psi}{\partial D}, \frac{\partial\Psi}{\partial\phi}, \frac{\partial\Psi}{\partial A_1}$. These specify the WFE caused by small deviations in duty cycle, phase, and amplitude, respectively. Furthermore, a variation in wavelength introduces an additional error in the wavefront phase calculation, where the phase

$$\Phi = \frac{2\pi}{\lambda}(n-1)t, \tag{5}$$

adds a wavelength dependency to each of the sensitivity functions. The model is extended with the introduction of the wavefront sensitivity function $\partial\Psi/\partial\lambda$, which for the zero and nonzero orders are as follows:

$$\frac{\partial\Psi}{\partial\lambda} = \begin{cases} -\frac{2\pi A_1 D(n-1)t\cos\Phi}{\lambda^2(A_0(1-D)+A_1 D\cos\Phi} - \frac{2\pi A_1^2 D^2(n-1)t\sin\phi^2}{\lambda^2(A_0(1-D)+A_1 D\cos\Phi)^2} = \frac{2\pi A_1 D(n-1)t(-A_1 D+A_0(D-1)\cos\Phi)}{\lambda^2(A_0-A_0 D+A_1 D\cos\Phi)^2}, & m=0, \\ \frac{2\pi A_1(n-1)t\cos\Phi}{\lambda^2(-A_0+A_1\cos\Phi)} - \frac{2\pi A_1^2(n-1)t\sin\phi^2}{\lambda^2(-A_0+A_1\cos\Phi)^2} = -\frac{2\pi A_1(n-1)t(A_1-A_0\cos\Phi)}{\lambda^2(A_0-A_1\cos\Phi)^2}, & m\neq 0. \end{cases} \tag{6}$$

To simplify these equations, it can be assumed that $A_0 = A_1 = 1$, if the CGH is used in transmission with uniform light irradiance. Additionally, the binary pattern on a CGH often has a duty cycle of $D = 0.5$. These assumptions simplify the sensitivity functions to:

$$\frac{\partial\Psi}{\partial\lambda} = \begin{cases} \frac{2\pi(1-n)t}{\lambda^2(1+\cos\Phi)}, & m = 0, \\ -\frac{\pi(n-1)t\left(\csc\frac{\Phi}{2}\right)^2}{\lambda^2}, & m \neq 0. \end{cases} \tag{7}$$

These parametric models allow a method to calculate phase changes in the wavefront that result from wavelength variations. The various sensitivity functions are evaluated directly to estimate the WFE due to small variations in duty cycle D, etch depth t, amplitude A_1, and wavelength λ. These functions are defined as follows: $\Delta W_D = \frac{1}{2\pi}\frac{\partial\Psi}{\partial D}\Delta D$, $\Delta W_\phi = \frac{\partial\Psi}{\partial\phi}\Delta\phi$, $\Delta W_{A_1} = \frac{1}{2\pi}\frac{\partial\Psi}{\partial A_1}\Delta A_1$, $\Delta W_\lambda = \frac{1}{2\pi}\frac{\partial\Psi}{\partial\lambda}\Delta\lambda$, respectively, where ΔD is the duty-cycle variation across the grating pattern; ΔW_D is the wavefront variation in waves due to

duty-cycle variation; $\Delta\phi$ is the etching depth variation in radians across the grating; ΔW_ϕ is the wavefront variation in waves due to etching depth variation; ΔA_1 is the amplitude variation; ΔW_{A_1} is the wavefront variation in waves due to amplitude variation; $\Delta\lambda$ is the wavelength variation; and ΔW_λ is the wavefront variation in waves due to wavelength variation.

The impact of the wavelength variation in the WFIRST grism metrology case using wavelength-tuning was estimated using the wavelength sensitivity functions. With a wavelength of $\lambda = 1550$ nm, it is assumed that the phase CGH receives uniform light irradiance in both etched and unetched regions, meaning $A_0 = A_1$. Additionally, the binary pattern on the CGH was measured such that the duty cycle was $D = 50\% \pm 1\%$, and the etch depth t was also measured to be 1.7 μm on average, with a variation of ~60 nm.

Depending on the instrument and testing configuration, most wavelength variations on interferometers will be confined to no more than 0.2 nm. However, due to the large cavity size of the WFIRST grism elements test setup, the wavelength varied only $\Delta\lambda = 0.01$ nm. Additionally, the CGHs were designed to use their first-diffraction order, making $m = 1$ in Eq. (4). Therefore, the WFE associated with using the CGHs to test the WFIRST grism elements can be obtained from Eq. (7). The WFE calculated from the sensitivity function is $\Delta W_\lambda = \frac{1}{2\pi}\frac{\partial\Psi}{\partial\lambda}\Delta\lambda$, where

$$\frac{\partial\Psi}{\partial\lambda} = -\frac{\pi(1.44402-1)(1.7\ \mu\text{m})(1.00084)^2}{(1.55\ \mu\text{m})^2}, \tag{8}$$

making $\Delta W_\lambda = -2.44$ pm when multiplied by 1550-nm wavelength, which is negligible in the total CGH errors.

If the wavelength sensitivity functions defined in Eq. (7) are studied more closely, over a 2-nm wavelength range, it can be observed that the sensitivity for the nonzero order is much less sensitive than that of the zero-order. For a wavelength variation of $\Delta\lambda = 0.01$ nm from the reference wavelength of 1550 nm, the WFE introduced for the zero-order case is $\Delta W_\lambda = -1.45$ nm, unlike the case for the nonzero order, where $\Delta W_\lambda = -2.44$ pm. This latter result is much less sensitive. Figure 6 shows the wavefront sensitivity function $\frac{\partial\Psi}{\partial\lambda}$ for both the zero-order and nonzero order cases, as shown in Eq. (7).

3.2 *WFIRST CGH Wavefront Error Simulation for Wavelength-Tuning Interferometry*

Two optical simulation studies were performed to cross-check the fidelity of the parametric model and to numerically estimate the WFEs caused by a wavelength variation of 2 nm (i.e., ± 1 nm from the nominal wavelength) using the Zemax$^+$ CGH models of the WFIRST grism elements E1 and E3. These studies show the effect that the wavelength variation for a 360-mm long cavity has on the CGH phase in the measurement of each of the grism elements. It is important to note that when using a wavelength-tuning interferometer, the amount of wavelength variation will depend on the testing configuration (cavity length), as discussed in Sec. 1.2.

Figure 7 shows the simulated WFEs of the CGH measuring E1 and E3 when varying the wavelength of ± 1 nm. The nominal wavelength that used to model the CGH test setups was 1550 nm, which is the wavelength of the interferometer used in the measurement. By design, a zero WFE was found at the nominal wavelength, as expected. To the right and left of that minimum, the wavelength varied up to 1 nm, making the full wavelength range of 1549 to 1551 nm.

These simulations confirm what the parametric sensitivity models in Sec. 3.1 indicate. The impact of wavelength variation is negligible since the sensitivity to wavelength variation for the nonzero case, where $m = 1$ in Eq. (4), is of the order of picometers. For a wavelength change of 0.01 nm from nominal, the parametric sensitivity model-based WFE was -2.44 pm from the wavelength sensitivity function defined in Eq. (7). The optical simulation study results in Fig. 7 show that the WFE equals ≈0.15 nm for a 0.01-nm wavelength change when the first order was used in the WFIRST grism CGH test. Since the ray-trace simulations model the actual testing conditions much better, including the retrace error and effects of the grism diffractive elements, these results are more precise. However, this still confirms a good agreement between the parametric estimate and the case-by-case numerical simulation outcomes.

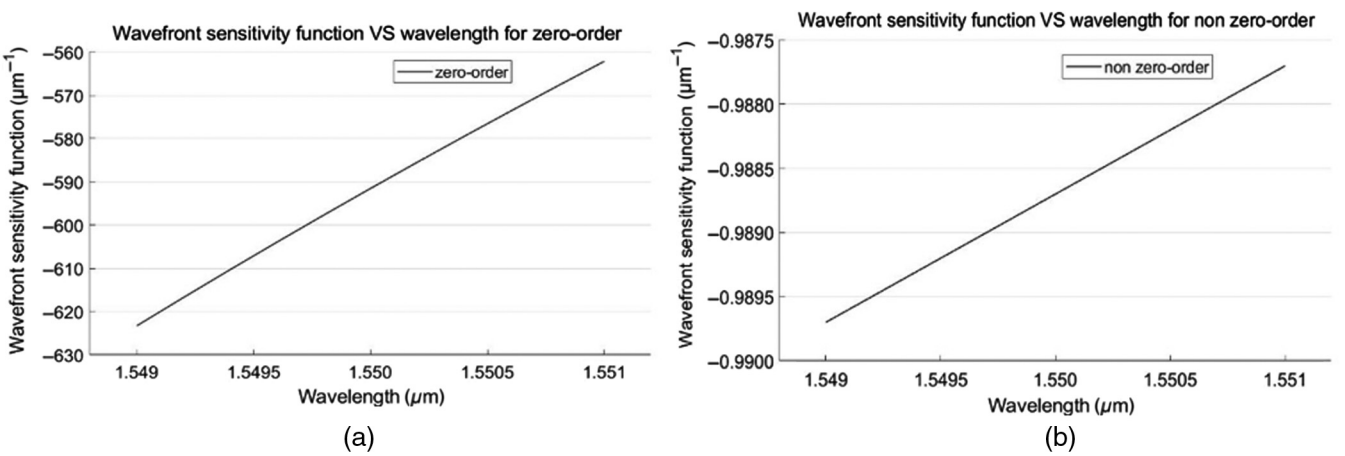

Fig. 6 Analytical results of the wavefront sensitivity function $\frac{\partial\Psi}{\partial\lambda}$ versus wavelength over a 2-nm range for the (a) zero-order and (b) nonzero order.

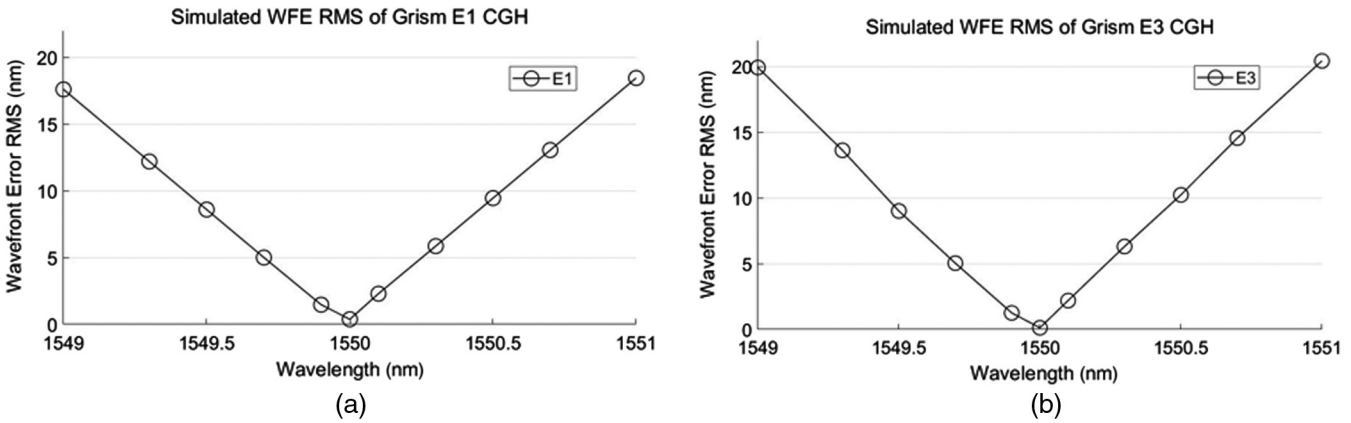

Fig. 7 Numerical simulation result showing the WFE as a function of wavelength variation over a 2-nm range for the phase CGHs designed to measure the WFIRST grism elements (a) E1 and (b) E3.

4 WFIRST Grism Test Results Using Infrared Wavelength-Tuning Interferometry

The designed infrared phase CGHs were manufactured and used to measure the actual WFIRST grism prototype elements. In an effort to verify that the wavelength-tuning capability was equivalent to the conventional piezo-shifting technique, the IR^3 interferometer at the National Institute of Standards and Technology (NIST) was used during this WFIRST grism testing campaign. This instrument was originally developed for thickness variation measurements of silicon wafers.[17] Unlike a typical interferometer, it has both wavelength-tuning and mechanical piezo-shifting capabilities at 1550 nm with a 152.4-mm diameter transmission flat. Both E1 and E3 were measured in collimated space in a double pass setup with a return flat after the test element. Figure 8 shows the E3 test layout with the IR^3 (the layout for E1 requires swapping the grism element and its corresponding CGH).

The IR^3 interferometer is a configurable tool, which can be used in two ways, as a Fizeau or Twyman–Green interferometer. In the Fizeau configuration, the interferometer can introduce phase-shifting via wavelength-tuning. Allowing the interferometric cavity to be fixed in size, making it unaffected by vibration and turbulence. The Twyman–Green configuration is used when the Fizeau mode cannot or when the cavity exceeds the tuning range of the laser source. In this case, phase shifting is implemented by mechanically moving the reference mirror with a piezoelectric shifter.[18]

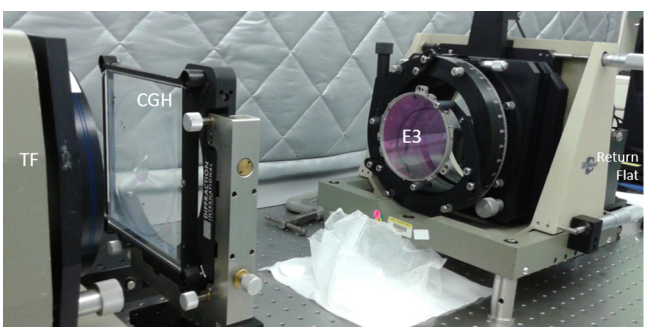

Fig. 8 Test setup of WFIRST grism prototype element E3 using the wavelength-tuning/piezo-shifting IR^3 interferometer. IR^3 collimator is to the left of the picture.

A lot of commercial interferometers that exist today introduce the phase variation via mechanically shifting the reference mirror. However, since grism testing required a more vibration insensitive instrument, a wavelength-tuning phase shift was better suited for this. Yet, a verification, where both phase-shifting techniques were appropriate due to the wavelength sensitivity nature of the parts, was needed, creating the necessity to compare both techniques.

Once the grism element and the CGH were placed and aligned in the layout shown in Fig. 8, without altering the test configuration, the interferometer measured the wavefront first by varying the wavelength and second by introducing a piezo-mechanical shift in the position of the transmission flat. The IR^3 uses a single-mode tunable diode laser with a wavelength range centered at 1550 nm. The piezo-mechanical shifter had a range of about 420-deg phase shift at 1550 nm, sufficient for basic phase-shifting algorithms. The mechanical phase shifting used seven phase steps with a 60-deg phase shift between them. Phase decoding was done using the Larkin–Oreb algorithm. When doing wavelength-tuning, a phase shifting algorithm with 13 steps and 60-deg phase increment between the steps was used.[19,20] As mentioned earlier, due to the 360-mm cavity length, the wavelength change required for the 720-deg phase shift was only ≈0.01 nm.

It has been reported in the literature that binary phase CGHs can have up to 40.5%[13,14] diffraction efficiency at the first orders. To verify the uniformity of the CGHs made for E1 and E3 testing, various random locations on the CGH were measured for etch depth and period; to verify that these should meet the required diffraction efficiency, they met specifications within <10%.

IR^3 measured the full aperture of the elements. Because of its dual phase-shifting capability, it could cross-check the insignificant WFE predicted during wavelength-tuning with results obtained using piezo-mechanical shifting. The wavefront measurement results from IR^3 shown in Fig. 9 indicate that both techniques yielded matching results for E1 and E3, within approximately a nanometer.

Table 3 compares the average WFEs over five measurements for both E1 and E3 and it demonstrates that wavelength-tuning for a long optical path length works as well as mechanical phase-shifting methods. The ≈0.01-nm wavelength shift during the wavelength-tuning process

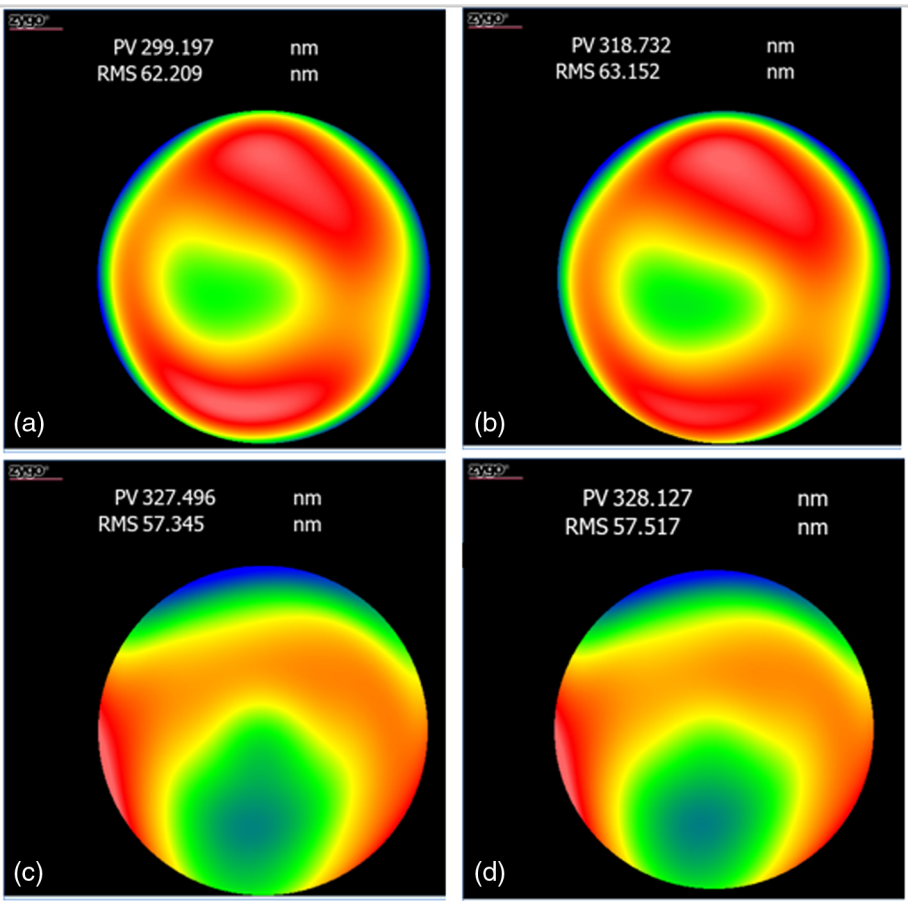

Fig. 9 Measured WFE maps for E1 and E3. (a) E1 measurement via piezo-shifting. (b) E1 measurement via wavelength-tuning. (c) E3 measurement via piezo-shifting. (d) E3 measurement via wavelength-tuning.

Table 3 Measured WFE RMS of the WFIRST grism elements E1 and E3 with the IR[3] interferometer.

	Phase-shifting technique	Wavelength-tuning	Mechanical piezo-shifting
Grism E1	Measured WFE RMS	63.1 ± 0.9 nm	62.2 ± 1.1 nm
Grism E3	Measured WFE RMS	57.5 ± 0.6 nm	57.3 ± 0.8 nm

successfully measured the WFIRST grism elements and did not impact the WFE, as modeled and simulated in Sec. 3.

Figure 10 shows a comparison of the measured Zernike fringe coefficients (from RMS normalized Z1 to Z25), via wavelength-tuning and piezo-shifting. These various coefficients are the result of the fitted wavefront maps, as shown in Fig. 9. They indicate how both measuring techniques essentially yield matching results, both in WFE RMS and fitted Zernike fringe coefficients. Figure 10 indicates that the discrepancy between the two IR[3] measurement techniques is

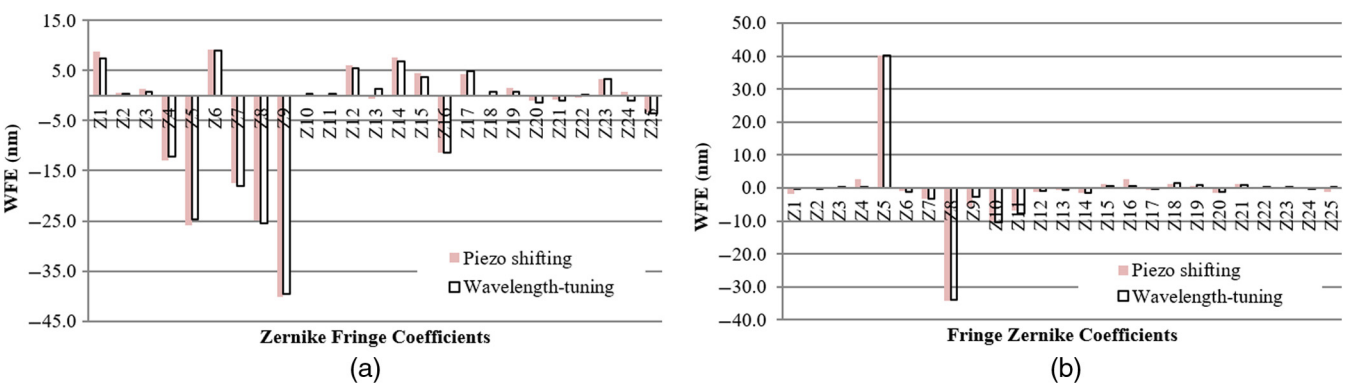

Fig. 10 Zernike fringe coefficient (RMS normalized) comparison between piezo-shifting and wavelength-tuning techniques, from Z1 to Z25 of the measured wavefront for (a) E1 and (b) E3.

negligible. The infrared wavelength-tuning interferometry for the WFIRST grism test CGH was successfully verified and the CGH low estimate error models and simulation studies agree with the measured performance.

5 Conclusion

This paper discusses the design strategy and manufacturing process of an infrared CGH. It also presents a developed parametric model, which enables an estimation of the wavefront phase error due to wavelength variations as part of the testing error, which can occur when using a wavelength-tuning interferometer. Also, numerical simulations of the WFE expected for the E1 and E3 WFIRST grism CGH tests were completed and showed the small impact that wavelength variation has on the final measurement when varying the wavelength ± 1 nm for the given cavity length. This result is consistent with the calculated errors associated with the wavelength sensitivity function.

Additionally, it was shown that both piezo-shifting and wavelength-tuning measuring techniques used on the WFIRST grism testing with CGHs essentially yield matching results, both in WFE RMS and fitted Zernike fringe coefficients. The discrepancy between the measurements using the two phase-shifting techniques was negligible, and the infrared wavelength-tuning interferometry data successfully verified that the CGH phase error models and simulation studies agree with the measured performance.

Furthermore, these results successfully show the performance of E1 and E3 at 1.55 μm; however, since the wavelength range of the telescope covers 1.35 to 1.95 μm, additional testing of the image performance via phase retrieval at other wavelengths is still needed. As well as measuring the full field of the instrument, since only the center field position was measured in the presented results.

Disclosures

The full description of the procedures used in this paper requires the identification of certain commercial products and their suppliers. The inclusion of such information should not be construed as indicating that such products and suppliers are endorsed by NASA or NIST, or are recommended by NASA or NIST, or that they are necessarily the best materials or suppliers for the purposes described.

Acknowledgments

Manufacturing the CGHs was possible using facilities provided by NIST's Center for Nanoscale Science and Technology (CNST). Access to the CNST NanoFab has not only greatly shortened our test turnaround time, but also provided flexibility to control the manufacturing process and to reduce cost. Additionally, Johannes A. Soons (NIST) wrote the bulk of the software used to generate the CGH layout in GDS format and William Green (NASA) provided needed modifications to the code as well.

References

1. B. A. Pasquale et al., "Optical design of WFIRST/AFTA wide-field instrument," in *Optical Society of America Technical Digest* (2014).
2. M. C. Noecker et al., "Coronagraph instrument for WFIRST-AFTA," *J. Astron. Telesc. Instrum. Syst.* **2**(1) 011001 (2016).
3. S. D. Office, "Wide-field infrared survey telescope astrophysics focused telescope assets WFIRST-AFTA," NASAV (2015).
4. D. Content et al., "Wide-Field InfraRed Survey Telescope (WFIRST) 2.4-meter mission study," *Proc. SPIE* **8860**, 88600E (2013).
5. Q. Gong et al., "Design, fabrication, and test of WFIRST-AFTA grism assembly," NASA New Technology Report (NTR#: GSC-17334-1).
6. Q. Gong et al., "Wide-field infrared survey telescope (WFIRST) slitless spectrometer: design, prototype, and results," *Proc. SPIE* **9904**, 990412 (2016).
7. M. Z. Dominguez et al., "Infrared testing of the wide-field infrared survey telescope grism using computer generated holograms," in *Optical Society of America Technical Digest (online)*, p. 3, OSA (2017).
8. J. Burge, C. Zhao, and P. Zhou, "Interferometric testing of optical surfaces," in *Digital Optical Measurement, Techniques and Applications*, p. 42, P. Rastogi, Ed., Artech House Publishers, Norwood (2015).
9. L. L. Deck and J. A. Soobitsky, "Phase shifting via wavelength tuning in very large aperture interferometers," *Proc. SPIE* **3782**, 432–442 (1999).
10. S. Wada, K. Akagawa, and H. Tashiro, "Electronically tuned Ti:sapphire laser," *Opt. Lett.* **21**(10), 731–733 (1996).
11. ZEMAX, Optical Design Program, U. m., *Optical Design Program, User's Manual*, Zemax (2011).
12. E. P. Goodwin and J. C. Wyant, *Field Guide to Interferometric Optical Testing*, SPIE Press Book, Bellingham, Washington (2006).
13. G. Barbastathis and C. Sheppard, "MIT open courseware," Retrieved from Lecture 16: Gratings: amplitude and phase, sinusoidal and binary, https://ocw.mit.edu/courses/mechanical-engineering/2-71-optics-spring-2009/video-lectures/lecture-16-gratings-amplitude-and-phase-sinusoidal-and-binary/
14. S. Tao, X. C. Yuan, and W. C. Cheong, "Comparison of amplitude- and phase-holograms," *Proc. SPIE* **4594** (2001).
15. P. Zhou and J. H. Burge, "Optimal design of computer-generated holograms to minimize sensitivity to fabrication errors," *Opt. Express* **15**, 15410–15417 (2007).
16. C. Zhao and J. H. Burge, "Optical testing with computer generated holograms: comprehensive error analysis," *Proc. SPIE* **8838**, 88380H (2013).
17. U. Griesmann et al., "Manufacture and metrology of 300 mm silicon wafers with ultra-low thickness variation," *American Institute of Physics, Characterization and Metrology for Nanoelectronics, Int. conf. Frontiers of Characterization and Metrology*, AIP, Washington, DC (2007).
18. Q. Wang, U. Griesmann, and R. Polvani, "Interferometric thickness calibration of 300 mm silicon wafers," *Proc. SPIE* **6024**, 602426 (2005).
19. K. G. Larkin and B. F. Oreb, "Design and assessment of symmetrical phase-shifting algorithms," *J. Opt. Soc. Am. A* **9**(10), 1740–1748 (1992).
20. J. Burke, "Phase decoding and reconstruction," in *Optical Methods for Solid Mechanics: A Full–Field Approach*, pp. 83–139, Wiley-VCH, Weinheim, Germany (2012).

Margaret Z. Dominguez received her BS in physics from the Universidad de las Americas Puebla in 2009. She is currently a PhD candidate at the College of Optical Sciences at the University of Arizona, while working full time at the optics branch at NASA Goddard Space Flight Center. She is currently working on the grism instrument on board the Wide-Field Infrared Survey Telescope (WFIRST), its assembly, alignment, and testing.

Catherine T. Marx is a senior optical designer and associate branch head at NASA Goddard Space Flight Center. She is currently working as a lead on the wide-field instrument on the WFIRST.

Qian Gong is a senior optical designer at NASA Goddard Space Flight Center. She is currently working on a variety of space telescope missions and proposals, including the WFIRST.

John G. Hagopian is a senior optical engineer at NASA Goddard Space Flight Center. He is currently working on a variety of space telescope missions and proposals, including the WFIRST.

Ulf Griesmann is a physicist in the surface and nanostructure metrology group in the engineering physics division of the Physical Measurement Laboratory (PML) at the National Institute of Standards and Technology (NIST). He is currently a chair of the optical fabrication and testing conference (OSA).

James H. Burge is an emeritus professor of optical sciences at the University of Arizona. He is an OSA and SPIE member. His research interests are in optical system engineering, including optical design, optomechanics, pointing and tracking, detectors, cryogenic systems; optical testing and precision metrology; fabrication of aspheric surfaces; development of ultra-lightweight mirrors for space; design and

fabrication of diffractive optics; stellar interferometry; and astronomical instrumentation.

Dae Wook Kim is an assistant professor of optical sciences and astronomy, University of Arizona. His main research area covers the precision freeform optics fabrication and metrology, such as interferometric system using computer-generated hologram, direct curvature measurement, and dynamic deflectometry system. He is currently a chair of the optical manufacturing and testing conference (SPIE) and the optical fabrication and testing conference (OSA). He has been serving as an associate editor for *Optics Express* journal.